Controlled Normal and Inverse Current-Induced Magnetization Switching and Magnetoresistance in Magnetic Nanopillars

M. AlHajDarwish,[1] H. Kurt,[1] S. Urazhdin,[1] A. Fert,[2] R. Loloee,[1] W. P. Pratt, Jr.,[1] and J. Bass[1]

[1]*Department of Physics and Astronomy, Center for Sensor Materials, Center for Fundamental Materials Research, Michigan State University, East Lansing, Michigan, USA 48824-2320*

[2]*Université Paris-Sud and Unite Mixte de Physique, CNRS/THALES, Orsay, France 91404*

(Received 19 December 2003; published 5 October 2004)

By combining pairs of ferromagnetic metals with the same or different signs of scattering anisotropies in ferromagnetic-nonmagnetic-ferromagnetic metal nanopillars, we independently invert just the magnetoresistance, just the direction of current-induced magnetization switching, or both together, at room temperature (295 K) and at 4.2 K. In all cases studied, the switching direction is correctly predicted from the net scattering anisotropy of the fixed ferromagnet, including both bulk and interfacial contributions.

DOI: 10.1103/PhysRevLett.93.157203 PACS numbers: 75.75.+a, 73.40.–c, 75.60.Jk, 75.70.Cn

The magnetization of a ferromagnetic (F) metal can be reversed by spin transfer from a spin-polarized current, i.e., without using a magnetic field [1–3]. Such current-induced magnetization switching (CIMS) [1–20] is seen in ($F1$-N-$F2$) nanopillars where a spin-polarized current prepared with a thicker layer $F1$ passes through a nonmagnetic metal (N) and switches the moment of a thinner layer $F2$. CIMS is promising for switching small magnetic devices (e.g., magnetic random-access memory), and also raises subtle fundamental issues.

Although CIMS is expected to result from spin polarization of the current, it has yet to be shown that CIMS can be manipulated (e.g., inverted) by changing that polarization. In prior studies, minority electrons were scattered more strongly in $F1$, $F2$ and at $F1$-N and N-$F2$ interfaces (positive spin anisotropy). The current is then positively spin polarized in the F layers, i.e., carried mainly by majority electrons. In such "standard" conditions, electrons flowing from $F1$ to $F2$ (negative charge current, $I < 0$) switch the moment **M2** of $F2$ from antiparallel (AP) to **M1** (high resistance R) to parallel (P) to **M1** (low R). Conversely, positive I (>0) switches $F2$ from P to AP. We call these behaviors "normal" CIMS and normal current-perpendicular-to-plane (CPP) magnetoresistance (MR).

We present CIMS experiments exploiting the possibility of inverting the spin anisotropy by doping $F1$, $F2$, or both together, with an impurity (Cr) that scatters majority spin electrons more strongly [21–28]. We thus show, for the first time, that inversion of the spin anisotropy can invert the CIMS direction, i.e., invert the signs of I for AP to P and P to AP transitions. We also find inversions of the MR (larger R for the P state) with appropriately doped samples, as expected from prior CPP-MR results at low temperature [21,22]. Measurements at 295 and 4.2 K show that the qualitative behaviors of both CIMS and MR are independent of temperature over this range.

Analysis of the switching behaviors lets us discriminate between models of CIMS. We divide the standard models of spin-transfer torque (STT) used to describe CIMS into two classes, ballistic [1,2,12] and diffusive [3,4,15,16,19]. Both predict that changing scattering anisotropies can invert the MR and/or CIMS. However, their expectations need not agree. In ballistic transport, the spin anisotropy comes only from reflections at the F-N interfaces. Inverting CIMS is predicted to require negative anisotropy at $F1$-N [12]. Inverting the MR should require opposite scattering anisotropies at $F1$-N and N-$F2$ [21]. In diffusive transport, the spin anisotropy of scattering within the F layers is also important, so that one must consider the net anisotropy of each F layer (i.e., the resultant effect of the bulk of F and its F-N interface). An additional effect, spin accumulation, can either support or compete with the effect of polarized current [3,4,15,16,19]. In addition to determining the relation between spin anisotropies and CIMS direction, we answer four questions relevant to understanding CIMS. (a) Is the CIMS direction set only by interface scattering anisotropy? No. (b) Can impurity scattering within the layers be important? Yes. (c) Do the anisotropies of $F1$ and $F2$ play different roles for the CIMS direction of $F2$? Yes. (d) Can spin accumulation be important? Yes.

To determine how changing spin anisotropies changes CIMS directions, we combine in different ways three pairs of materials: Py-Cu (Py = $Ni_{84}Fe_{16}$), with both bulk and interface anisotropies positive [21]; Fe(Cr)-Cr [Fe(Cr) = $Fe_{95}Cr_5$], with both negative [22–28]; and Ni(Cr)-Cu [Ni(Cr) = $Ni_{97}Cr_3$], with thick enough Ni(Cr) so its negative anisotropy dominates the positive anisotropy of the interface [29]. The net anisotropy is found using the MR. Comparing Fe(Cr)-Cr with Ni(Cr)-Cu for $F1$ or $F2$ tests the importance of interface anisotropies. Table I lists the signs for $F1$, $F2$ bulk, $F1$-N, N-$F2$ interfaces, and $F1$(net), $F2$(net), as well as for the observed MR and CIMS.

 © 2004 The American Physical Society

TABLE I. *F*1-*N*-*F*2 for each figure, giving the spin anisotropies (+ = positive, − = negative) of *F*1, *F*1-*N*, and their net anisotropy *F*1(Net), those of *F*2, *N*-*F*2, and their net anisotropy *F*2(Net), and the signs of the observed MR and CIMS (+ = normal and − = inverse).

Figure	*F*1-*N*-*F*2	*F*1	*F*1-*N*	*F*1(Net)	*F*2	*N*-*F*2	*F*2(Net)	MR	CIMS
1	Py-Cu-Py	+	+	+	+	+	+	+	+
2	Fe(Cr)-Cr-Fe(Cr)	−	−	−	−	−	−	+	−
3	Py-Cu-Cr-Fe(Cr)	+	+	+	−	−	−	−	+
4	Ni(Cr)-Cu-Py	−	+	−	+	+	+	−	−
5	Py-Cu-Ni(Cr)	+	+	+	−	+	−	−	+

Our sample preparation and measurement techniques are described in Ref. [20]. Our multilayers are triode sputtered onto Si substrates, and patterned into nanopillars of roughly elliptical shape and dimensions $\sim$70 nm $\times$ 130 nm. The samples consist of a thick Cu lower contact, the multilayer, and a thick Au top contact. The *N* layer is made thick (6–20 nm) to minimize exchange coupling between *F*1 and *F*2. To simplify switching, samples are ion milled only through *F*2 and part of *N*, leaving *F*1 (fixed polarizer) to have a much larger area ($\sim \mu m^2$) and be thicker than *F*2. Dipolar coupling between *F*1 and *F*2 is then minimal, and *H* (along the easy axis) reverses **M1** and **M2** sequentially, but *I* reverses only **M2** of *F*2 (free switcher). For each sample, the switching directions of MR and CIMS are the same at 295 and 4.2 K. Each switching behavior was independently reproduced, and no inconsistent switching was seen.

Py and Py-Cu interfaces both have positive scattering anisotropy [21]. In accord with prior data [20], Fig. 1 shows that Py(24)-Cu(10)-Py(6) nanopillars (layer thicknesses in nm) give normal MR and normal CIMS. At both 295 and 4.2 K, the MR transitions from P to AP occur after *H* passes through zero, consistent with little or no magnetic coupling. The agreement between minimum and maximum values of dV/dI for the MR and CIMS curves shows that the switching is complete. Figures 2–5 also show weak coupling and complete switching.

In contrast to Py and Py-Cu, Fe(Cr) and Fe-Cr interfaces both have negative scattering anisotropies [22–28]. Since *F*1 and *F*2 are the same alloy, Fe(Cr)(30)-Cr(6)-Fe(Cr)(3.5) nanopillars should give normal MR [21,22]. Figure 2 shows that they do and also give inverse CIMS; see also [23]. The changes in dV/dI vs *I* or *H* are smaller than for Py-Cu-Py, due to spin-memory loss in the Cr(6) layer [24] and smaller scattering anisotropy of Fe(Cr) [22].

Figure 3 shows data for the four component system Py(20)-Cu(7)-Cr(3)-Fe(Cr)(3). Combining net positive anisotropy for *F*1 with net negative for *F*2 gives the expected inverse MR [21,22]. But the CIMS is normal—$I > 0$ switches from P to AP—since inverse MR means the largest resistance in the P state.

Figure 4 shows the fourth case, Ni(Cr)(20)-Cu(20)-Py(10). Combining net negative anisotropy for Ni(Cr) with net positive anisotropy for Py gives the expected inverse MR, and now inverse CIMS.

Figure 5 shows another way to achieve inverse MR with normal CIMS, using Py(24)-Cu(10)-NiCr(4). In Figs. 3 and 5, this same combination of MR and CIMS occurs with opposite *F*2 interface anisotropies—negative in Fig. 3 but positive in Fig. 5.

Last, in Figs. 2 and 4, opposite interface anisotropies for *F*1 do not change the CIMS direction.

Before comparing our data with theory, we summarize the results in Figs. 1–5. As expected for the MR [21,22], when the net scattering anisotropies for *F*1 and *F*2 are the same (Figs. 1 and 2), the MR is normal, and when they are opposite (Figs. 3–5), the MR is inverse. New for CIMS, when the net scattering anisotropy for *F*1 is positive, CIMS is normal (Figs. 1, 3, and 5), and when it is negative (Figs. 2 and 4), CIMS is inverse. For these samples, the direction of CIMS is set by the net scattering anisotropy of *F*1 and is independent of that of *F*2. Comparing Figs. 3 and 5, and Figs. 2 and 4, shows that, when bulk scattering

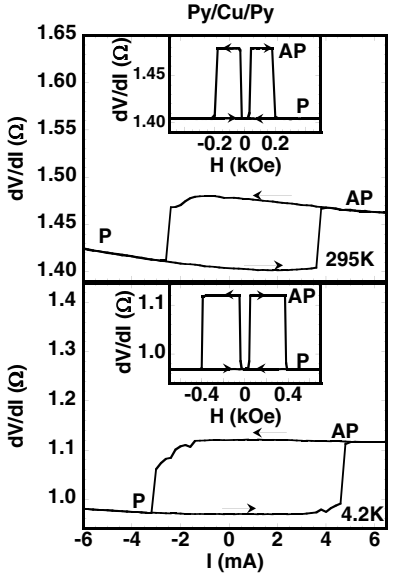

FIG. 1. Py(24)-Cu(10)-Py(6) data at 295 K (top) and 4.2 K (bottom) showing normal MR (dV/dI vs *H* at $I = 0$) in the insets and normal CIMS for dV/dI vs *I* in the main figures at $H = 0$ Oe for 295 K and at $H = 20$ Oe for 4.2 K. In all figures, $I > 0$ is always from *F*1 to *F*2.

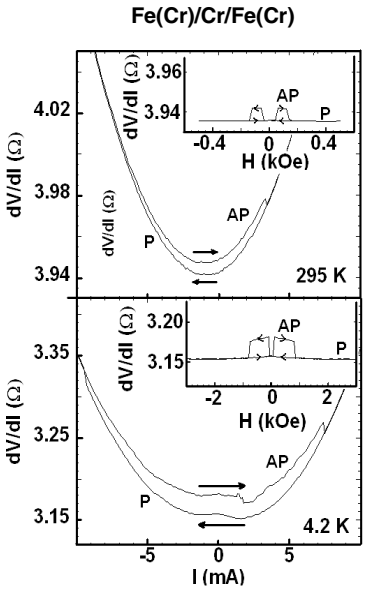

FIG. 2. Fe(Cr)(30)-Cr(6)-Fe(Cr)(3.5) data at 295 K (top) and 4.2 K (bottom) showing normal MR (dV/dI vs H at $I = 0$) in the insets but inverse CIMS for dV/dI vs I at $H = 0$ in the main figures.

predominates, the CIMS direction is independent of the scattering anisotropy of $F1$-N and N-$F2$. Finally, dominance of the bulk contribution of scattering anisotropy in either $F1$ [e.g., Ni(Cr) in Fig. 4] or $F2$ [Ni(Cr) in Fig. 5] is inconsistent with ballistic transport through the nanopillar, where the interfaces must dominate the scattering. While ballistic STT models cannot describe our data involving Ni(Cr), the CIMS directions in Figs. 1–5 accord

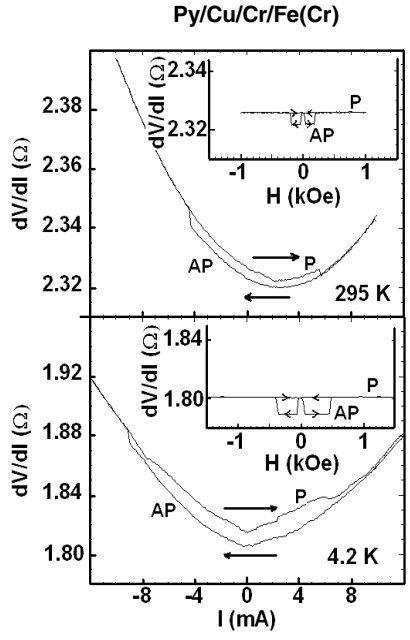

FIG. 3. Py(20)-Cu(7)-Cr(3)-Fe(Cr)(3) data at 295 K (top) and 4.2 K (bottom) showing inverse MR (dV/dI vs H at $I = 0$) in the insets but normal CIMS for dV/dI vs I at $H = 0$ in the main figures.

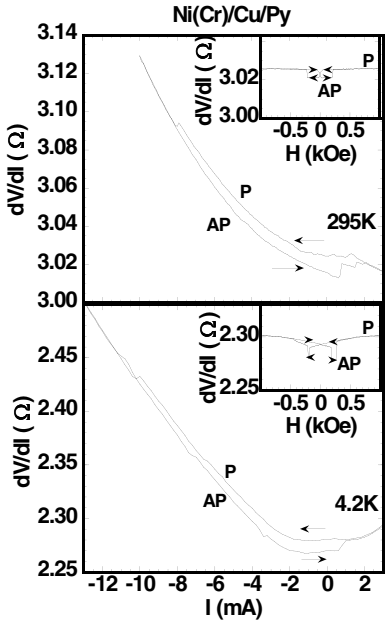

FIG. 4. Ni(Cr)(20)-Cu(20)-Py(10) data at 295 K (top) and 4.2 K (bottom) showing inverse MR (dV/dI vs H at $I = 0$) in the insets and inverse CIMS for dV/dI vs I at $H = 0$ in the main figures.

with the ballistic prediction of [12] if the scattering anisotropy at the $F1$-N interface is simply replaced by the net anisotropy for $F1$.

For diffusive transport, the current polarization in N depends upon the net scattering anisotropies of both $F1$ and $F2$, and CIMS depends upon both the spin-polarized charge current and spin-accumulation effects [3,4,15,19]. Equation (1) reproduces Eq. 5 of Ref. [19] for the torque Γ^{P} at a small angle from the P state (for Γ^{AP}, replace P by AP). Our notations for $F1$ and $F2$ are reversed from [19].

$$\Gamma^{\mathrm{P}}/\hbar = [\{(\nu_F m_N^{\mathrm{P}})/8 + (j_{m,N}^{\mathrm{P}})/2\}(1 - e^{-t_N/\lambda_N}) + \{(\nu_F m_{F1}^{\mathrm{P}})/4 + j_{m,F1}^{\mathrm{P}}\}e^{-t_N/\lambda_N}] \times [\hat{M}_2 \times (\hat{M}_2 \times \hat{M}_1)]. \quad (1)$$

Equation (1) comes from an extension of the Valet-Fert

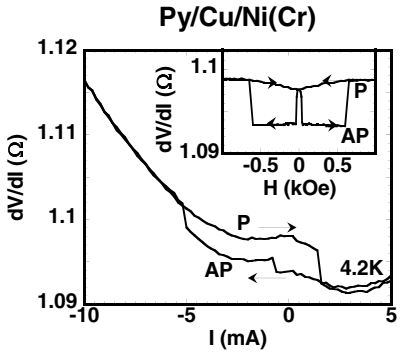

FIG. 5. Py(24)-Cu(10)-Ni(Cr)(4) data at 4.2 K showing inverse MR (dV/dI vs H at $I = 0$) in the inset and normal CIMS for dV/dI at $H = 0$ Oe in the main figure.

[30] model of CPP-MR to noncollinear states. ν_F is the Fermi velocity in N, m_N^{P} and $j_{m,N}^{\mathrm{P}}$ are the spin-accumulation density [15,16,19,30] and spin-current density in N just outside the $F2$-N interface calculated for the P state, m_{F1}^{P} and $j_{m,F1}^{\mathrm{P}}$ are the same quantities in $F1$ just inside the $F1$-N interface, t_N and λ_N are the thickness and mean-free path of N, and $\hat{M}$ is a unit vector in the direction of $\mathbf{M}$. The second set of $\{\}$ braces dominates the usual case when $t_N \ll \lambda_N$ and the first dominates if $t_N \gg \lambda_N$. The signs of spin current and spin accumulation can support each other or compete.

Using the best parameters from CPP-MR experiments [21,24,29], we calculate spin currents and spin accumulations [21,30], and insert them into Γ^{P} or Γ^{AP}. Except for Fig. 4, the signs of spin current and accumulation always agree and are as expected from the sign of the net spin anisotropy of $F1$ seen by MR. The case for Fig. 4 is more complex. For P to AP, the spin accumulation dominates Γ^{P} and gives the observed inverse CIMS at $I < 0$; due to the particular parameters of Ni(Cr) and Py, the spin current alone would predict normal CIMS. For AP to P, the spin current dominates Γ^{AP} and gives the observed inverse CIMS at $I > 0$. Thus, we reproduce the behaviors in Fig. 4.

To summarize, we have shown that judiciously chosen pairs of ferromagnetic metals or alloys can produce all four combinations of normal and inverse MR and current-induced magnetization switching at both 4.2 and 295 K. The MR is normal if the net scattering anisotropies of $F1$ and $F2$ have the same sign, and inverse if they do not. For the samples studied, the CIMS direction is set solely by the net anisotropy for $F1$, although in Fig. 4 this result requires dominance of spin accumulation for the P to AP transition. This latter result, as well as the inverted MRs in Figs. 4 and 5, show that the interpretation of MR and CIMS must generally take account not only of the interface scattering assumed in ballistic models but also the scattering (and diffusion) within the F layers. As the widely accepted mechanism of CIMS is a quasi-interfacial absorption of the transverse component of the spin current [1,12,15,19], the importance of scattering within the F layers might seem surprising. However, in a noncollinear magnetic configuration, the transverse spin current in the frame of $F2$ is related to the longitudinal one in $F1$, and a global treatment [15,19] of the longitudinal and transverse components of the spin current and spin accumulation requires the diffusive aspects of the CPP-MR theory [21,30].

The authors thank Henri Jaffrès for spin-accumulation calculations, and N. O. Birge, P. M. Levy, and M. D. Stiles for helpful suggestions. This research was supported by the MSU CFMR, CSM, Keck Microfabrication Facility, NSF Grants No. DMR 02-02476, No. 98-09688, NSF-EU collaborative Grant No. 00-98803, and Seagate Technology.

[1] J. Slonczewski, J. Magn. Magn. Mater. **159**, L1 (1996).
[2] L. Berger, Phys. Rev. B **54**, 9353 (1996).
[3] J. Slonczewski, J. Magn. Magn. Mater. **247**, 324 (2002).
[4] L. Berger, J. Appl. Phys. **89**, 5521 (2001).
[5] M. Tsoi *et al.*, Phys. Rev. Lett. **80**, 4281 (1998); **81**, 493(E) (1998); Nature (London) **406**, 46 (2000).
[6] E. B. Myers *et al.*, Science **285**, 867 (1999).
[7] J. A. Katine *et al.*, Phys. Rev. Lett. **84**, 3149 (2000).
[8] J. Grollier *et al.*, Appl. Phys. Lett. **78**, 3663 (2001); Phys. Rev. B **67**, 174402 (2003).
[9] For additional experimental references see J. Bass *et al.*, Phys. Status Solidi (a) **201**, No. 7, 1379 (2004).
[10] Ya. B. Bazaliy *et al.*, Phys. Rev. B **57**, R3213 (1998).
[11] A. Brataas *et al.*, Phys. Rev. Lett. **84**, 2481 (2000).
[12] X. Waintal *et al.*, Phys. Rev. B **62**, 12 317 (2000).
[13] C. Heide *et al.*, Phys. Rev. B **63**, 064424 (2001); C. Heide, Phys. Rev. Lett. **87**, 197201 (2001).
[14] Y. Tserkovnyak *et al.*, Phys. Rev. B **66**, 224403 (2002).
[15] M. D. Stiles and A. Zangwill, J. Appl. Phys. **91**, 6812 (2002); Phys. Rev. B **66**, 014407 (2002).
[16] S. Zhang *et al.*, Phys. Rev. Lett. **88**, 236601 (2002).
[17] J.-E. Wegrowe *et al.*, Europhys. Lett. **45**, 626 (1999); J. Appl. Phys. **91**, 6806 (2002).
[18] S. Urazhdin, Phys. Rev. B **69**, 134430 (2004).
[19] A. Fert *et al.*, J. Magn. Magn. Mater. **272–276**, 1706 (2004).
[20] S. Urazhdin *et al.*, Phys. Rev. Lett. **91**, 146803 (2003); Appl. Phys. Lett. **83**, 114 (2003).
[21] J. Bass and W. P. Pratt, Jr., J. Magn. Magn. Mater. **200**, 274 (1999).
[22] C. Vouille *et al.*, Phys. Rev. B **60**, 6710 (1999).
[23] M. AlHajDarwish *et al.*, J. Appl. Phys. **95**, 6771 (2004).
[24] A. Zambano *et al.*, J. Magn. Magn. Mater. **253**, 51 (2002).
[25] I. Mertig *et al.*, J. Magn. Magn. Mater. **151**, 363 (1995).
[26] I. A. Campbell and A. Fert, in *Ferromagnetic Materials*, edited by E. P. Wolforth (North-Holland, Amsterdam, 1982), Vol. 3, pp. 747.
[27] M. D. Stiles and D. R. Penn, Phys. Rev. B **61**, 3200 (2000).
[28] K. Xia *et al.*, Phys. Rev. B **63**, 064407 (2001).
[29] W. Park *et al.*, J. Appl. Phys. **85**, 4542 (1999).
[30] T. Valet and A. Fert, Phys. Rev. B **48**, 7099 (1993).